



# Modeling of gas saturation based on acoustic wave and pore structure classification and application in the low-porosity and low-permeability reservoir

Weibiao Xie<sup>1,2,3</sup> · Qiuli Yin<sup>3</sup> · Guiwen Wang<sup>1,2</sup> · Wei Guan<sup>3</sup> · Zhiyong Yu<sup>3</sup>

Received: 9 February 2021 / Accepted: 13 May 2021 / Published online: 18 May 2021  
© Saudi Society for Geosciences 2021

## Abstract

Gas saturation is an essential parameter in natural gas reservoir evaluation. As complex pore structure reduces the resistivity contrast between gas and water layers, gas saturation is difficult to calculate accurately by rock resistivity in low-porosity and low-permeability reservoir. The gas saturation is positively correlated with the relative value of compressional wave (P wave) slowness' square based on the rock acoustic wave theory. In this study, rock samples are divided into four types of pore structures according to nuclear magnetic resonance (NMR) data. Relation models between the gas saturation and the relative value of P wave slowness' square are established for each type. New models are further applied in field logging data in low-porosity and low-permeability gas-bearing sandstone reservoirs. The result shows that the new models calculated gas saturation is in good agreement with the gas-producing test. This paper provides a new way of qualitative evaluation of gas saturation. It enriches effective evaluation methods in low-porosity and low-permeability gas-bearing reservoirs with non-electrical logging data.

**Keywords** P wave and S-wave slowness · Low-porosity and low-permeability reservoir · Gas saturation · Pore structure classification

## Introduction

Natural gas reservoir becomes explore hotspot in recent years (Hosseini et al. 2013; Tamaki et al. 2016). Gas saturation is a crucial parameter in natural gas reservoirs, and it is a basic data of research works of reserve calculation and exploitation plan (Kadkhodaie-Ilkhchi et al. 2014; Yan et al. 2013; Zhao et al. 2020). At present, the gas saturation is mainly calculated by rock resistivity methods (Xu et al. 2015; Junchang et al.

2011; Wang Xiujuan et al. 2010) and non-electrical methods (Hongxia et al. 2015; Fattahi and Karimpouli 2016; Sambo et al. 2018; Mollison et al. 1999).

Acoustic logging data is one of the non-electric methods to estimate the gas saturation (Yuguang et al. 2008; Gaowei et al. 2014; Lucier et al. 2011). Many researchers have carried out fundamental researches in rock acoustic theory (Dutta and Seriff 1979; Dutta 2012) and rock acoustic experiments (Gist 1994; Endres and Knight 1991; Uyanik 2019). Brie et al. (1995) has proposed the cross plot of the compressional wave (P wave) slowness and the velocity ratio of P wave and shear wave (S-wave) to predict gas content (Brie et al. 1995; Keys and Xu 2002). Smith and Yafei (1987) have proposed a method of identifying the fluid property using P wave and S-wave data (Smith and Gidlow 1987; Yafei 1999). Haines et al. (2020) have reported a gas saturation estimation method by acoustic log data in the Hydrate Stratigraphic (Haines et al. 2020). Shi et al. (2019) have studied quantitative evaluation of the porosity and the gas saturation, and qualitative identification of the lithology, the gas potential, and the fracture effectiveness of shale gas reservoirs by dipole array acoustic logging (Wenrui et al. 2019). Dugarov et al. (2019) have reported acoustic velocity models for samples bearing hydrates of

Responsible Editor: Santanu Banerjee

- ✉ Weibiao Xie  
gareth123@126.com
- ✉ Guiwen Wang  
wanggw@cup.edu.cn

- <sup>1</sup> State Key Laboratory of Petroleum Resources and Prospecting, China University of Petroleum (Beijing), Beijing 102249, China
- <sup>2</sup> College of Geosciences, China University of Petroleum (Beijing), Beijing 102249, China
- <sup>3</sup> PetroChina Jidong Oilfield Company, Tangshan 063004, Hebei, China

different types (Dugarov et al. 2019). Liu et al. (2019) have reported a new method of estimating the free-to-adsorbed ratio in shale gas reservoirs using acoustic amplitude attenuation (Kun et al. 2017). Moreover, many scholars have carried out research works on the relationship between water saturation and acoustic velocity (King et al. 2000; Khaksar et al. 1999; Na'imi et al. 2014; Morgan et al. 2012).

However, the measured acoustic velocity is affected by many factors (White 1975; Dehua et al. 1986; Sams and Andrea 2001; Jixin et al. 2004). The pore structure is an important influencing factor (Neithalath et al. 2005; El-Husseiny et al. 2019; Li Tianyang et al. 2020; Amalokwu et al. 2015). Junbao et al. (2019) have discussed the effect of different saturation degrees and the micro-pore characteristics on the longitudinal wave velocity (Wang Junbao et al. 2019). Lee and Waite (2008) have reported a velocity-based estimation method of the pore-space gas hydrate saturation (Lee and Waite 2008). Sun et al. (2002) have introduced the formation geometrical as a factor to characterize the pore structure's influence on the wave velocity (Sun et al. 2002). Si et al. (2016) and Siggins and Dewhurst (2003) have discussed the influence of the saturation, the pore pressure on the sandstone acoustic properties (Wenpeng et al. 2016; Siggins and Dewhurst 2003). The influence of pore structure needs to be fully considered in the acoustic method of gas saturation calculation.

The low-porosity and low-permeability sandstone reservoirs have various pore structure types according to mercury injection and nuclear magnetic resonance (NMR) data (Zhao et al. 2016a, b, Zhao et al. 2017; Xie et al. 2021; Wang and Li 2008; Liang et al. 2016; Endres and Knight 1991). It is necessary to consider the pore structure's influence on the relationship between the acoustic characteristics and the gas saturation. To achieve the purpose of quantitative evaluation of the gas saturation in the low-porosity and low-permeability sandstone reservoir, the paper has divided the rock samples into four types of pore structures according to the NMR experimental data. The relationship models between the gas saturation and the acoustic wave characteristics have been established for each pore structure type. Further, new models have been applied in field logging data to verify the accuracy of gas saturation calculation. The new method provides a reference for gas-bearing identification in tight sandstone and carbonate reservoir.

### Modeling of gas saturation

Under the assumption that the rock is homogeneous and isotropic, the Gassmann equation is a relationship model among the bulk modulus of fluidsaturated rock, the bulk modulus of dry rock, porosity and the bulk modulus of pore fluid. It has ignored the effect of fluid's relative motion and rockskeleton

on wave propagation in fluid-saturated rock (Gassmann 1951; Han and Batzle 2004).

Based on the Gassmann equation, when pores are saturated with two-phase fluids (gas and water), the rock bulk modulus can be depicted as follows.

$$K(S_g) = K_{dry} + \frac{(1-K_{dry}/K_{ma})^2}{S_g \phi \left( \frac{1}{K_g} - \frac{1}{K_w} \right) + \frac{\phi}{K_w} + \frac{1-\phi}{K_{ma}} + \frac{K_{dry}}{K_{ma}^2}} \quad (1)$$

where  $K_{ma}$ (Gpa) is the bulk modulus of rock matrix,  $K_{dry}$ (Gpa) is the bulk modulus of dry rock,  $K$ (Gpa) is the bulk modulus of water-saturated rock, and  $K_f$ (Gpa) is the bulk modulus of water in pores.  $\phi$ (v/v) is the porosity.  $S_g$ (v/v) is the gas saturation, and  $K_g$ (Gpa) and  $K_w$ (Gpa) are the bulk modulus of natural gas and water, respectively.  $\mu$ (Gpa) and  $\mu_{dry}$ (Gpa) are the shear modulus of water-saturated rock and dry rock, respectively.

According to Eq. (1), the gas saturation can be obtained.

$$S_g = \frac{\Delta K(S_g)^{-1} - \Delta K(S_g = 0)^{-1}}{\Delta K(S_g = 1)^{-1} - \Delta K(S_g = 0)^{-1}} \quad (2)$$

The equivalent P wave velocity and the equivalent S-wave velocity are expressed as follows (Gist 1994).

$$\begin{cases} v_p = \sqrt{\frac{K + \frac{4}{3}\mu}{\rho}} \\ v_s = \sqrt{\frac{\mu}{\rho}} \end{cases} \quad (3)$$

where  $\rho$  (kg/m<sup>3</sup>) is the density of the water-saturated rock. It can be seen that the compressional wave correlates with the gas saturation, while the transverse wave does not correlate with the gas saturation.

According to Eq. (3), the ratio of the P wave velocity and the S-wave velocity is obtained.

$$vpvs = \frac{v_p}{v_s} = \sqrt{\frac{K}{\mu} + \frac{4}{3}} \quad (4)$$

where  $K$  is the function of the gas saturation; we can write  $vpvs$  as a function of  $S_g$ ; then Eq. (4) can be written as

$$K(S_g) = \mu \left\{ [vpvs(S_g)]^2 - \frac{4}{3} \right\} \quad (5)$$

Based on Eq. (5),  $\Delta K(S_g)$  in Eq. (2) can be rewritten as

$$\Delta K(S_g) = \mu \left\{ [vpvs(S_g)]^2 - [vpvs(S_g = 1)]^2 \right\} \quad (6)$$

Due to the shear wave having no relation with the gas saturation  $S_g$ , so Eq. (6) can be rewritten as

$$\Delta K(S_g) = \mu \left[ \frac{v_p^2(S_g) - v_p^2(S_g = 1)}{v_s^2} \right] \tag{7}$$

From Eq. (7), we can obtain

$$\Delta K(S_g) \propto v_p^2(S_g) = [DTC(S_g)]^{-2} \tag{8}$$

By substituting Eq. (8) into Eq. (2), we can obtain

$$S_g \propto \frac{DTC(S_g)^2 - DTC(S_g = 0)^2}{DTC(S_g = 1)^2 - DTC(S_g = 0)^2} \tag{9}$$

Define  $\Delta DTC^2 = \frac{DTC(S_g)^2 - DTC(S_g=0)^2}{DTC(S_g=1)^2 - DTC(S_g=0)^2}$ , where  $\Delta DTC^2$

is the relative value of the P wave slowness' square.  $DTC(S_g = 0)(\mu s/ft)$  is the P wave slowness in 100% water-saturated rocks.  $DTC(S_g = 1)(\mu s/ft)$  is the P wave slowness in dry rocks.

Equation (9) reveals a positive relationship between the gas saturation and the relative value of P wave slowness' square.

### Verification and modeling of $S_g$ based on pore structure classification

In this study, 23 representative rock samples selected from Shahejie Formation, Paleogene system, Nanpu sag, China, are prepared to do acoustic experiments. The rock samples are fine sandstone with few clays and belong to braided river delta front sedimentary facies. The experimental apparatus employed in this study included Panametrics high-pressure pulse generator/receiver, 1 MHz longitudinal and transverse acoustic transducer and Hewlett Packard (HP) digital storage oscilloscope. For each core, the P wave velocity and the S-

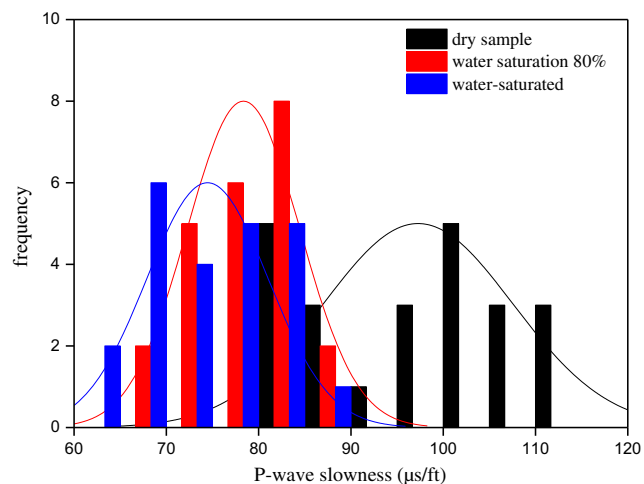


Fig. 1 P wave slowness distribution under different saturated states

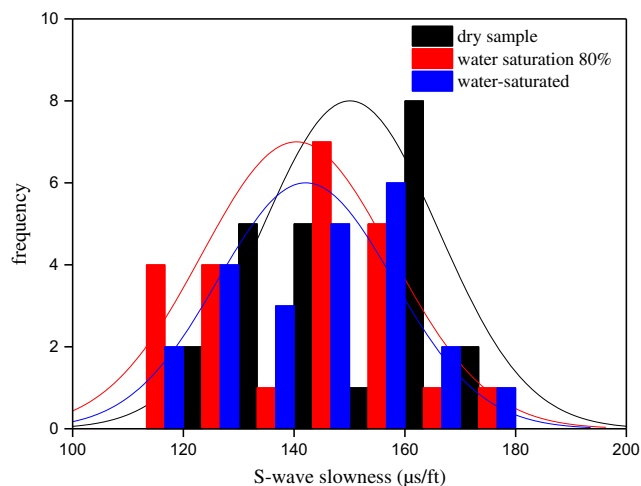


Fig. 2 S-wave slowness distribution under different saturated states

wave velocity are measured under dry state, 100% water saturated state and different gas saturation state, respectively.

Figure 1 shows histograms of P wave slowness distribution under 100% water-saturated state (blue), 80% water saturation state (red), and dry state (black). Figure 2 shows histograms of S-wave slowness' distribution under 100% water-saturated state (blue), 80% water saturation state (red), and dry state (black).

Comparing Fig. 1 and Fig. 2 shows that the P wave slowness distribution range changes much more than the S-wave slowness distribution range under different water-saturated states. P wave slowness gets smaller when water saturation gets higher; however, S-wave slowness has no noticeable change.

According to the experimental data, a cross plot between the P wave slowness' square and the gas saturation is established, as shown in Fig. 3. The gas saturation has a positive relationship with  $\Delta DTC^2$ . The gas saturation calculation model is established.

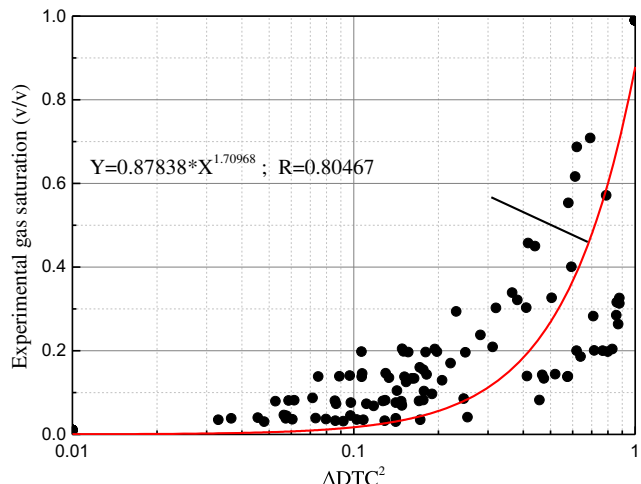
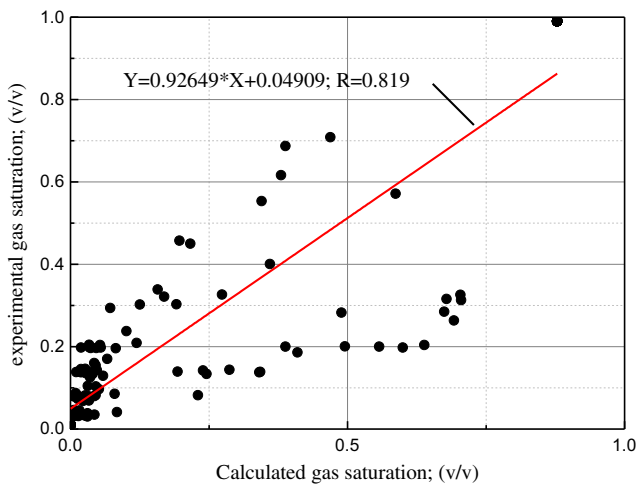


Fig. 3 Gas saturation models with non-pore structure classification



**Fig. 4** The result of calculated gas saturation models with non-pore structure classification

$$S_g = 0.87838(\Delta DTC^2)^{1.70968} \quad R = 0.80467 \quad (10)$$

Figure 4 shows the comparison between the experimental gas saturation and the gas saturation calculated by Eq. (10). The fitting relationship between the calculated gas saturation and the experimental values is  $y = 0.92649x + 0.04909$ ; the goodness of fit  $R = 0.819$ . The average relative error of calculated gas saturation is 69.7%. The low accuracy of the model (as shown in Eq.(10)) limits its practical application.

According to the NMR experimental data of 20 rock samples selected from those 24 acoustic experimental rock samples, the pore structure is divided into four types. For these 20 rock samples, the average porosity is 9.5%, the average permeability is 0.123md, and the average irreducible water saturation is 62%. Table 1 shows each type’s characteristic parameters, and Fig. 5 shows each type’s representative T2 spectrum shapes. It can be seen that from type I to type IV, the average porosity, the average permeability, the large pore volume of the T2 spectrum, and the T2 spectrum’s geometric mean decrease and the average irreducible water saturation increases, indicating the pore structure becomes more complex.

According to each pore structure type’s experimental data of P wave velocity and S-wave velocity under different gas saturation states, the relationship models between the P wave slowness’ square and the gas saturation are established. Figure 6 shows the cross plot between the measured P wave slowness’ square and the experimental gas saturation.

Rock samples of type I and type II are mainly featured by large- and middle-size pore throat; the gas saturation has an excellent linear relationship with  $\Delta DTC^2$ . The gas saturation model for type I and II reservoir is established as follows.

$$S_g = 0.9928\Delta DTC^2 + 0.0018 \quad R = 0.9899 \quad (11)$$

Rock samples of type III are mainly featured by middle-size pore throat. The gas saturation has a good quadratic relationship with  $\Delta DTC^2$ . The gas saturation model for type III reservoir is established as follows.

$$S_g = 0.5727(\Delta DTC^2)^2 + 0.3836\Delta DTC^2 + 0.0184 \quad R = 0.9876 \quad (12)$$

Rock samples of type IV are mainly featured by small-size pore throat. The gas saturation has a good exponential relationship with  $\Delta DTC^2$ . The gas saturation model for type IV reservoir is established as follows.

$$S_g = 0.0206exp(3.517\Delta DTC^2) \quad R = 0.929 \quad (13)$$

Figure 7 shows the comparison between the experimental gas saturation and the gas saturation calculated using pore-structure classified gas saturation models. The fitting relationship between the calculated gas saturation and the experimental gas saturation is  $y = 1.0015x$ ; the goodness of fit  $R = 0.989$ . The average relative error of calculated gas saturation is 34%. Also, the average error of calculated gas saturation is 21% when the gas saturation is more than 20%.

### Application

The new method is applied in the reservoir of 4385–4420 m in Well ×85. The average porosity is 0.0875(v/v) and the average

**Table 1** Characteristic parameters of different types of pore structure

Types	Spectral characteristics	$\Phi$ (%)	K (mD)	T <sub>2AM</sub> (ms)	T <sub>2GM</sub> (ms)	Swi (%)
I	Unimodal or bimodal distribution T2 spectrum, large pore coarse throat structure	8.35~13.31 11.31	0.03~1.17 0.4119	11.67~39.25 20.24	43.72~131.93 66.84	29.13~59.98 46.96
II	bimodal distribution T2 spectrum, intermediate pore fine-coarse throat structure	5.08~9.27 7.42	0.05~0.13 0.0607	3.43~7.91 6.93	37.07~39.56 38.50	60.14~70.61 62.59
III	unimodal distribution T2 spectrum, intermediate pore medium throat structure	10.90~12.86 12.28	0.02~0.08 0.0558	6.13~7.59 6.24	16.90~19.65 18.05	59.97~67.73 63.63
IV	Unimodal distribution T2 spectrum, fine pore fine throat structure	5.00~8.48 6.95	0.003~0.007 0.0046	2.36~2.87 2.62	4.33~10.24 6.36	67.43~73.64 70.24

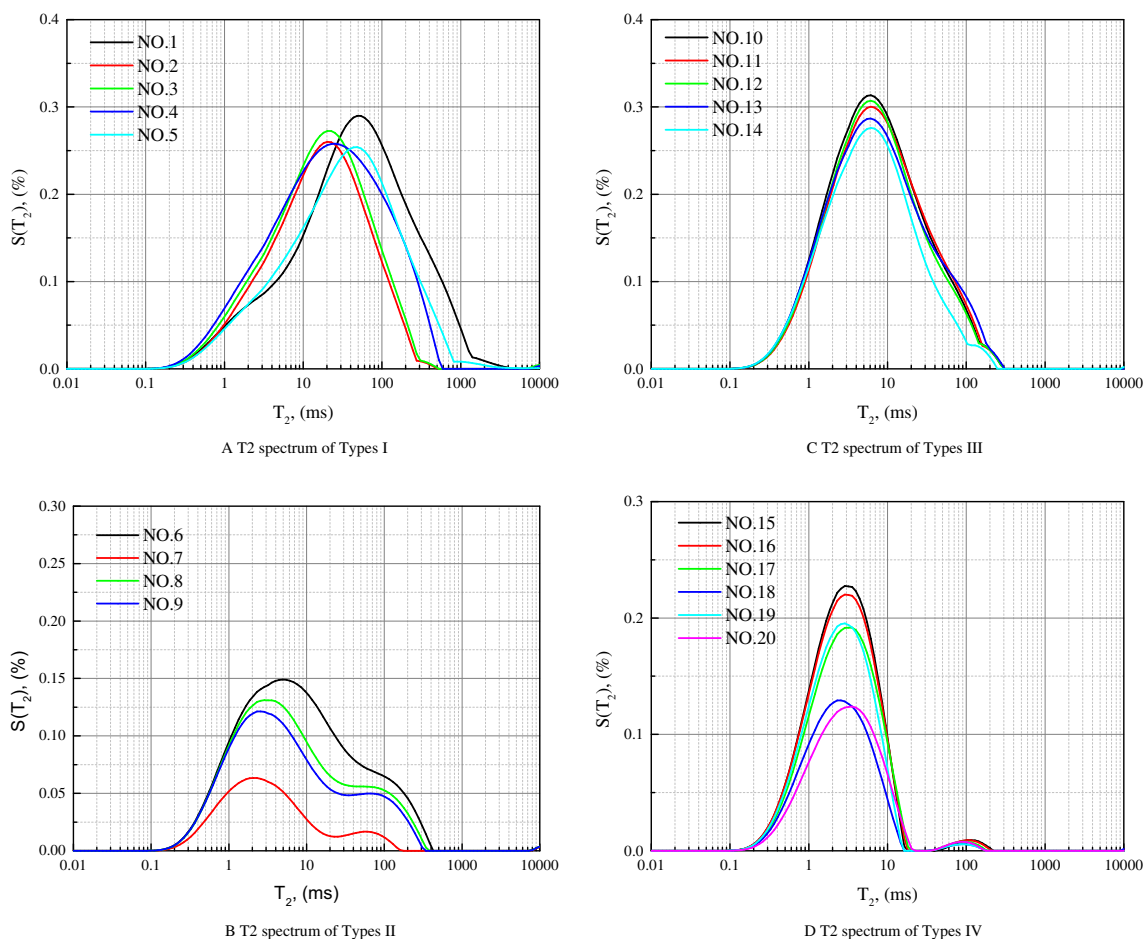


Fig. 5 Classification of rock samples by NMR

permeability is 0.6md, belonging to the low-porosity and a low-permeability reservoir.

In this section, according to the linear relationship between P wave slowness and S-wave slowness in both 100% water-saturated rocks and dry rocks, parameters  $DTC(S_g = 0)$  and  $DTC(S_g = 1)$  can be derived from Eq. (14) and Eq. (15).

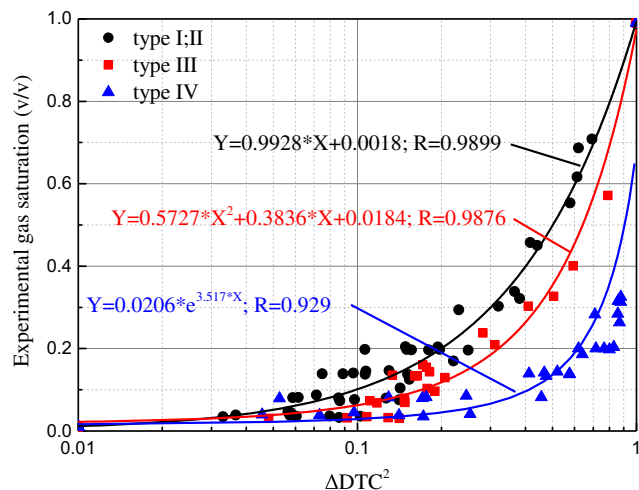


Fig. 6 Gas saturation models for different types

Figure 8 shows the cross plot between the P wave and the S-wave in 100% water-saturated rocks. Figure 9 shows the cross plot between the P wave and the S-wave in dry rocks. It can be seen clearly that under both states, relationships between the P wave slowness and the S-wave slowness are linear.

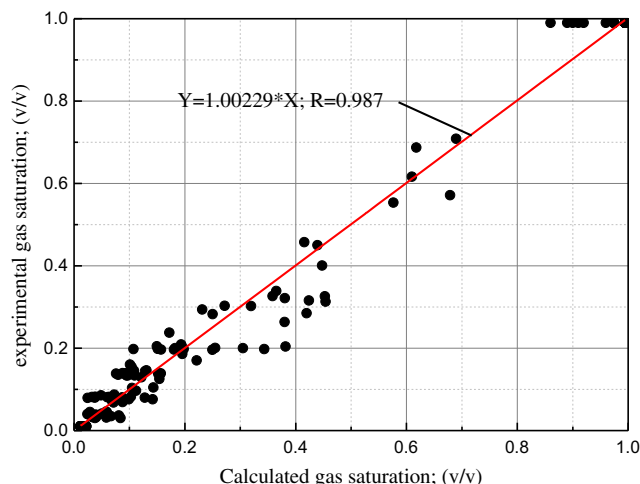
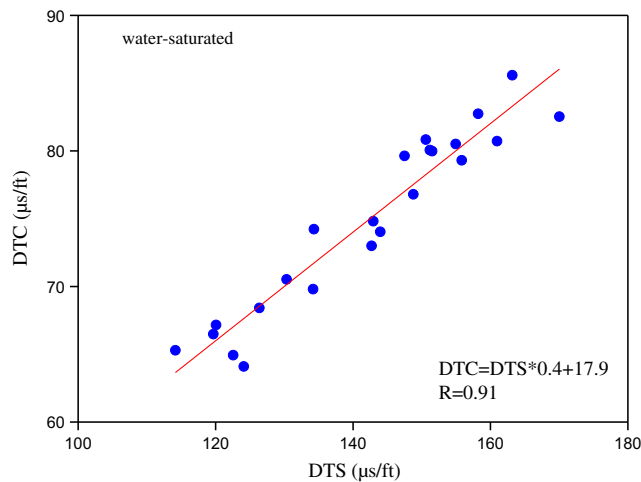


Fig. 7 Result of calculated gas saturation for classification



**Fig. 8** Crossplot between DTC and DTS in 100% saturated water rocks

The relationship between the P wave slowness and the S-wave slowness under 100% water-saturated is depicted as follows.

$$DTC(S_g = 0) = 0.4DTS + 17.9 \quad R = 0.91 \quad (14)$$

The relationship between the P wave slowness and the S-wave slowness in dry rocks is depicted as follows.

$$DTC(S_g = 1) = 0.63DTS + 3.4 \quad R = 0.87 \quad (15)$$

where  $DTC(\mu\text{s}/\text{ft})$  is the P wave slowness and  $DTS(\mu\text{s}/\text{ft})$  is the S-wave slowness.  $DTC(S_g = 0)(\mu\text{s}/\text{ft})$  is the P wave slowness in 100% water-saturated rocks.  $DTC(S_g = 1)(\mu\text{s}/\text{ft})$  is the P wave slowness in dry rocks.  $S_g(v/v)$  is the gas saturation.

Figure 10 shows the evaluation result using the pore structure classified gas saturation models. Track 1–12 includes conventional well logs, estimates of reservoir physical parameters, NMR logging T2 spectrum, compressional wave and shear wave data, water saturation calculated by Archie model, gas saturation calculated by

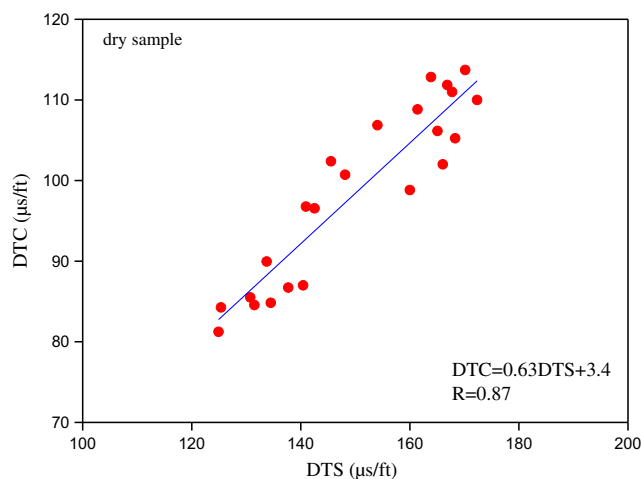


**Fig. 9** Crossplot between DTC and DTS in dry rocks

the new model and core measurements of bound water saturation. The calculation results of reservoir parameters are shown in Table 2. The gas saturation can be calculated by the Archie model ( $S_g = 1 - S_w$ ).

The result indicates that the trend of gas saturation is inversely related to shale content. The reservoir with high shale content has low gas saturation, and the reservoir with low shale content has high gas saturation. Furthermore, track 11–12 shows the comparison among the water saturation calculated by the Archie model, the gas saturation calculated by the new model, and the core measurements of the bound water saturation. The gas-producing test result of layer 5 and layer 6 ( $1 \times 10^4 \text{ m}^3$  per day gas without water) shows the reservoir has no movable water (mainly the irreducible water, the gas saturation is calculated by  $S_g = 1 - S_{irr}$ . And  $S_{irr}$  (v/v) is the irreducible water.) The gas saturation calculated using the new model is in good agreement with the gas saturation calculated by the core measurements. The average relative error of calculated gas saturation by the new model and the Archie model is 13.8% and 35.5%, respectively. The result of calculated gas saturation in Fig. 10 shows that the new model improves the accuracy of gas saturation calculation, and provides a reliable evaluation of gas saturation based on acoustic logging data.

## Discussion and future work

The new method needs acoustic logging data in its application. The radial detection depth of acoustic logging is shallow, so the accuracy of the new method is often affected by drilling mud filtrate intrusion and borehole conditions. The new model can calculate the gas saturation accurately in low-porosity and low-permeability reservoir, tight sandstone reservoir, or underbalanced drilling well that have little mud filtrate intrusion's influence. The new method can only be used as the indicator parameter of gas saturation in medium-high-porosity and medium-high-permeability reservoir.

Further research directions and subjects concerning the reservoir gas saturation and reservoir assessment may be anticipated in:

- a. a. For sandstone reservoirs with complex pore structures (Xie et al. 2020), there are various types of pore structures. Further study on pore structure classification method and gas saturation calculation model by pore structure classification is the key to improve the calculation accuracy of this paper's method.
- b. The pore structures of the natural gas reservoir in carbonate rock, volcanic rock, granite, and other lithologies are quite different from sandstone (Li and Zhang 2018;

**Table 2** Calculation results of reservoir parameters

Layer	RT (ohm m)	POR (%)	PERM (md)	Sw_Archie (v/v)	Sg (v/v)	Core sirr (v/v)	Pore structure types
1	38	10.1	0.08	0.65	0.25	–	III
2	16	4.3	0.01	1	0.03	–	IV
3	31	11.2	0.34	0.69	0.56	–	I
4	30	13.2	0.8	0.6	0.365	0.6	I
5	41	10.7	0.45	0.65	0.47	0.51	I
6	31	10.2	0.12	0.64	0.38	0.62	II
7	36	7.7	0.01	0.71	0.29	–	IV
8	31	6.5	0.01	1	0.07	–	IV

Zhonghong Chen et al. 2016). It is a new application work to establish the gas saturation model by this paper’s method.

- c. The estimation of total organic carbon content in the tight oil reservoir and shale oil reservoir is the key parameter of reservoir evaluation (Peiqiang Zhao

et al. 2016a, b; Linqi Zhu et al. 2018; Mahmood et al. 2018). The calculation of organic carbon content according to the response characteristics of acoustic logging is a new research method. The method presented in this paper can be used for reference in the calculation of organic carbon content.

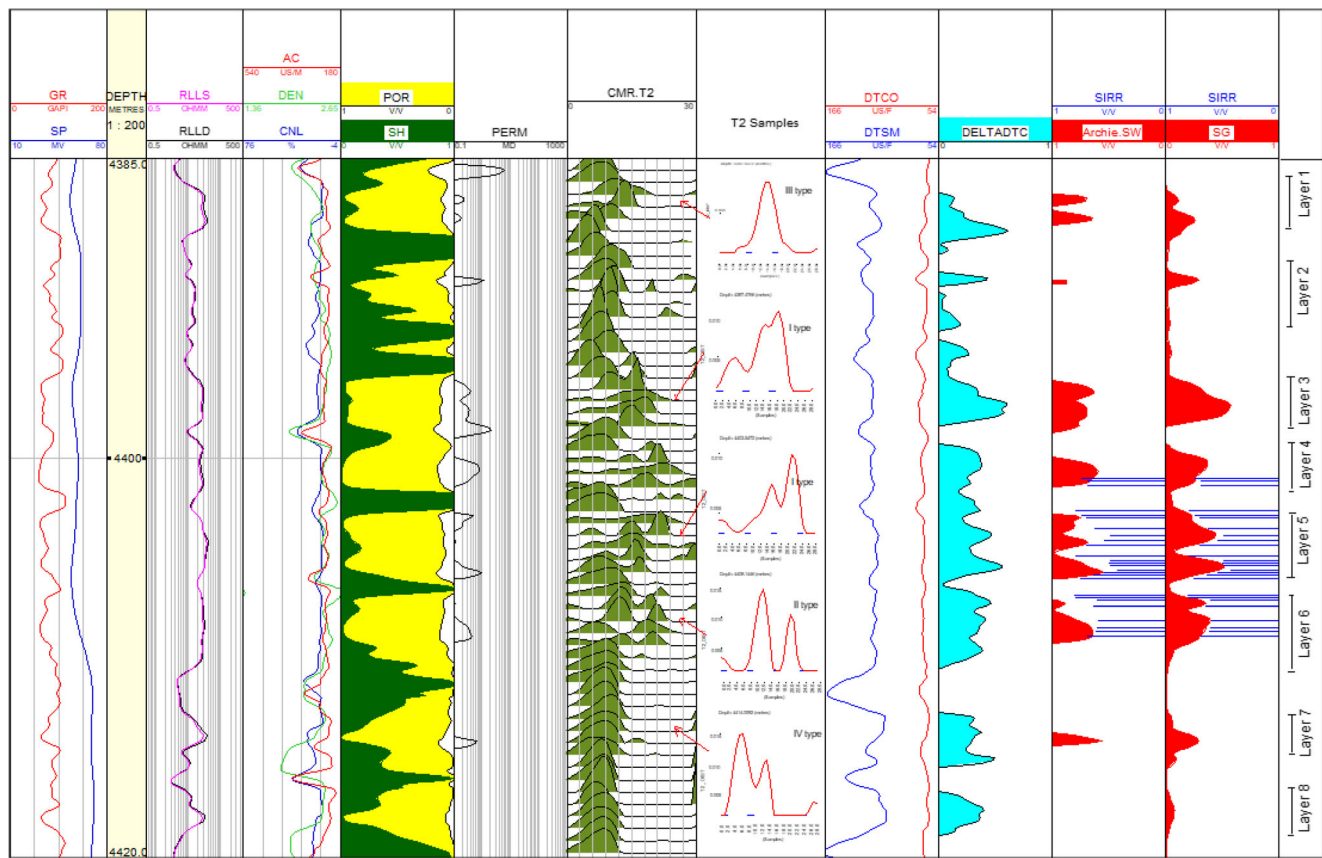


**Fig. 10** Application in well x85 (4385–4420 m). Tracks from left to right include track 1–6: natural gamma-ray logging (GR: API)/spontaneous potential logging (SP: MV), apparent resistivity logs (RLLD/RLLS: OHMM), acoustic-wave slowness logs (AC: us/m)/bulk density (DEN: g/cm<sup>3</sup>), neutron porosity (CNL: %), estimates of porosity (POR: %)/shale content (SH: %), estimates of permeability (PERM: md). Track 7–8: NMR logging T2 spectrum (CMR.T2: ms), T2 spectrum samples (T2

Samples.ms). Track 9–10: compressional wave (DTCO: us/ft) and shear wave (DTSM: us/ft), P wave slowness’ square (DELTADTC: none). Track 11: water saturation (Archie.SW: v/v) estimated using Archie model, measurements of bound water saturation (CORE-SIRR: v/v). Track 12: gas saturation (SG: v/v) estimated using pore structure classified gas saturation model and core measurements of bound water saturation (CORE-SIRR: v/v)

## Conclusion

In the low-porosity and low-permeability reservoir, pore structure greatly influences rock acoustic characteristics. The method in this paper can improve gas saturation calculation accuracy in low-porosity and low-permeability reservoir.

- (1) Based on acoustic theory, the gas saturation is positively correlated with the relative value of the P wave slowness' square.
- (2) The longitudinal wave correlates with the pores' gas saturation, while the transverse wave does not correlate with gas saturation.
- (3) In the low-porosity and low-permeability reservoir, pore structure greatly influences rock acoustic characteristics. According to NMR experimental data of 20 rock samples, the pore structure is divided into four types. For each pore structure type, gas saturation models are established. The comparison between experimental gas saturation and calculated gas saturation verifies the accuracy of the pore structure classified gas saturation model.
- (4) The pore structure classified gas saturation model is applied in logging data. The result is in good agreement with the core measurement result. The new method overcomes the limitation of using the resistivity saturation model to calculate gas saturation in the gas-bearing sandstone reservoir.
- (5) While pore structure is a comprehensive response of porosity, pore geometry, connectivity, rock minerals, etc., more attention should be paid to the pore structure classification methods using both NMR and mercury injection experimental data and further studies are needed to link the rock minerals to the acoustic properties.

## Declarations

**Conflict of interest** The authors declare that they have no competing interests.

## References

- Amalokwu K, Best AI, Chapman M, Minshull TA, Li X (2015) Partial gas saturation effects on P-wave anisotropy in porous rock with aligned fractures. *Seg Technical Program Expanded Abstracts*
- Brie A, Pampuri F, Marsala AF, et al. (1995) Shear sonic interpretation in gas bearing sands. SPE Annual Technical Conference and Exhibition. Dallas, Texas: Society of Petroleum Engineers
- Chen Z, Wang X, Zha M, Zhang Y, Cao Y, Yang D, Wu K, Chen Y, Yuan G (2016) Characteristics and formation mechanisms of large volcanic rock oil reservoirs: a case study of the carboniferous rocks in the Kebai fault zone of Junggar Basin, China. *AAPG Bull* 100(10):1585–1617
- Dehua H, Amos N, Dale M (1986) Effects of porosity and clay content on wave velocities in sandstones. *Geophysics*, 1986 51(11):2093–2107
- Dugarov GA, Duchkov AA, Duchkov AD, Drobchik AN (2019) Laboratory validation of effective acoustic velocity models for samples bearing hydrates of different type. *Journal of Natural Gas Science and Engineering* 63:38–46
- Dutta NC (2012) Attenuation and dispersion of compressional waves in fluid-filled porous rocks with partial gas saturation (white model)—part i: biot theory. *Geophysics* 44(11):1777
- Dutta NC, Seriff AJ (1979) On White's model of attenuation in rocks with partial gas saturation. *Geophysics* 44(11):1806–1812
- El-Husseiny A, Vega S, Nizamuddin S (2019) The effect of pore structure complexity and saturation history on the variations of acoustic velocity as function of brine and oil saturation in carbonates. *J Pet Sci Eng* 179:180–191
- Endres AL, Knight R (1991) The effects of pore-scale fluid distribution on the physical properties of partially saturated tight sandstones. *J Appl Phys* 69(2):1091–1098
- Fattahi H, Karimpouli S (2016) Prediction of porosity and water saturation using pre-stack seismic attributes: a comparison of Bayesian inversion and computational intelligence methods. *Comput Geosci* 20(5):1075–1094
- Gaowei H, Yuguang Y et al (2014) Acoustic response of gas hydrate formation in sediments from South China Sea. *Mar Pet Geol* 52:1–8
- Gassmann F (1951) Elastic waves through a packing of spheres. *Geophysics* 16(4):673–685
- Gist GA (1994) Interpreting laboratory velocity measurements in partially gas-saturated rocks. *Geophysics* 59(7):1100–1109
- Haines SS, Collett T, Boswell R, Lim TK, Okinaka N, Suzuki K, Fujimoto A (2020). Gas hydrate saturation estimation from acoustic log data in the 2018 Alaska North Slope Hydrate-01 Stratigraphic Test Well. Proc. ICGH-10, Singapore
- Han DH, Batzle ML (2004) Gassmann's equation and fluid-saturated effects on seismic velocities. *Geophysics* 69(2):398–405
- Hongxia M, Wei S, Wu P (2015) Application of nmr technology on test of movable fluid saturation of tight sandstone gas reservoir. *Adv Mater Res* 1092-1093:1361–1365
- Hosseini SE, Andwari AM, Wahid MA, Bagheri G (2013) A review on green energy potentials in Iran. *Renew Sust Energ Rev* 27:533–545
- Jixin D et al. (2004). Analysis of the velocity anisotropy and its affection factors in shale and mudstone. *Chinese J Geophys* 47(5): 862 868, doi: 10.3321/j. issn: 0001-5733. 2004, 05, 018. (In Chinese abstract)
- Junbao W, Zhenzhong R, Zhanping S, Runke H, Yang T (2019) Study of the effect of micro-pore characteristics and saturation degree on the longitudinal wave velocity of sandstone. *Arab J Geosci* 12(13):1–11
- Junchang S, Yang Z et al (2011) Study on distribution law of irreducible water and gas saturation of tight sandstone gas reservoir. *Shenzhen Daxue Xuebao (Ligong Ban)/Journal of Shenzhen University ence and Engineering* 28(5):377–383 (In Chinese abstract)
- Kadkhodaie-Ilkhchi R, Moussavi-Harami R, Rezaee R, Nabi-Bidhendi M, Kadkhodaie-Ilkhchi A (2014) Seismic inversion and attributes analysis for porosity evaluation of the tight gas sandstones of the whicher range field in the Perth basin, Western Australia. *Journal of Natural Gas Science & Engineering* 21:1073–1083
- Keys RG, Xu S (2002) An approximation for the xu-white velocity model. *Geophysics* 67(5):1406–1414
- Khaksar A, Griffiths CM, Mccann C (1999) Compressional- and shear-wave velocities as a function of confining stress in dry sandstones. *Geophys Prospect* 47:487–508
- King MS, Marsden JR, Dennis JW (2000) Biot dispersion for P and S wave velocity in partially and fully saturated sandstone. *Geophysical Prospecting*, 2000 48(6):1075–1089
- Kun L et al (2017) A new method for estimating the free-to-adsorbed ratio in shale gas reservoirs using acoustic amplitude attenuation and porosity. *J Geophys Eng* 14(5):1042–1051



- Lee MW, Waite WF (2008) Estimating pore-space gas hydrate saturations from well log acoustic data. *Geochem Geophys Geosyst* 9(7)
- Li H, Zhang J (2018) Well log and seismic data analysis for complex pore-structure carbonate reservoir using 3D rock physics templates. *J Appl Geophys* 151:175–183
- Xiao Liang, Mao Zhiqiang & Xie Xiuhong. 2016. A new method of evaluating tight gas sands pore structure from nuclear magnetic resonance (NMR) logs. EGU General Assembly Conference. EGU General Assembly Conference Abstracts
- Lucier AM, Hofmann R, Bryndzia LT (2011) Evaluation of variable gas saturation on acoustic log data from the Haynesville shale gas play, NW Louisiana, USA. *Lead Edge* 30(3):300–311
- Mahmood MF, Ahmad Z, Ehsan M (2018) Total organic carbon content and total porosity estimation in unconventional resource play using integrated approach through seismic inversion and well logs analysis within the Talhar shale, Pakistan. *Journal of Natural Gas Science and Engineering* 52:13–24
- Mollison RA, Schon JS, Fanini ON, Kreigshauser B, Meyer WH, Gupta PK (1999). A model for hydrocarbon saturation determination from an orthogonal tensor relationship in thinly laminated anisotropic reservoirs
- Morgan EC, Vanneste M, Lecomte I et al (2012) Estimation of free gas saturation from seismic reflection surveys by the genetic algorithm inversion of a P wave attenuation model [J]. *Geophysics* 77(4): R175–R187
- Na'imi SR, Shadizadeh SR, Riahi MA, Mirzakhani M (2014) Estimation of reservoir porosity and water saturation based on seismic attributes using support vector regression approach. *J Appl Geophys* 107:93–101
- Neithalath N, Marolf A, Weiss J, Olek J (2005) Modeling the influence of pore structure on the acoustic absorption of enhanced porosity concrete. *J Adv Concr Technol* 3(1):29–40
- Sambo, C. H. , Hermana, M. , Babasari, A. , Janjuhah, H. T. , & Ghosh, D. P. . (2018). Application of artificial intelligence methods for predicting water saturation from new seismic attributes. *Offshore Technology Conference Asia*
- Sams MS, Andrea M (2001) The effect of clay distribution on the elastic properties of sandstones. *Geophys Prospect* 49(1):128–150
- Siggins AF, Dewhurst DN (2003) Saturation, pore pressure and effective stress from sandstone acoustic properties. *Geophys Res Lett* 30(2)
- Smith GC, Gidlow PM (1987) Weighted stacking for rock property estimation and detection of gas. *Geophys Prospect* 35(9):993–1014
- Sun YF, Massaferro JL, Eberli G, Teng YC (2002). Quantifying the effects of pore structure and fluid saturation on acoustic wave velocity in carbonates. In *Theoretical And Computational Acoustics 2001* (pp. 335–347)
- Tamaki M, Suzuki K, Fujii T, Sato A (2016) Prediction and validation of gas hydrate saturation distribution in the eastern Nankai trough, Japan: geostatistical approach integrating well-log and 3D seismic data. *Interpretation* 4(1):SA83–SA94
- Tianyang L et al (2020) Numerical study of pore structure effects on acoustic logging data in the borehole environment. *Fractals* 28(03):2050049
- Uyanik O (2019) Estimation of the porosity of clay soils using seismic p- and s-wave velocities. *J Appl Geophys* 170:103832
- Wang K, Li N (2008) Numerical simulation of rock pore-throat structure effects on nmr t2 distribution. *Appl Geophys* 5(2):86–91
- Wenpeng S et al (2016) Experimental study of water saturation effect on acoustic velocity of sandstones. *Journal of Natural Gas Science and Engineering* 33:37–43
- Wenrui S et al (2019) Application of dipole array acoustic logging in the evaluation of shale gas reservoirs. *Energies* 12(20):3882
- White JE (1975) Computed seismic speeds and attenuation in rocks with partial gas saturation. *Geophysics* 40(2):224–232
- Xie W, Yin Q, Guan W, Wang G, Lai J (2020) Estimating the relative permeability from the electrical parameters of sandstone with a complex pore structure. *Energy&Fuels*. 2020;34,14124–34,14131
- Xie W, Yin Q, Wang G, Zhiyong Y (2021) Variable dimension fractal-based conversion method between the nuclear magnetic resonance T2 spectrum and capillary pressure curve. *Energy&Fuels*. 2021(35): 351–357
- Xiujuan W et al. (2010). Estimation of gas hydrate saturation based on resistivity logging and analysis of estimation error. *Geoscience*
- Xu D, Jianmeng S, Jun L, Gao H, Xuefeng L, Wang J (2015) Experimental research of gas shale electrical properties by NMR and the combination of imbibition and drainage. *J Geophys Eng* 12(4):610–619
- Yafei W (1999) Estimation of gas saturation using p-to-s converted waves. *Seg Technical Program Expanded Abstracts* 19(1):2484
- Yan BJ, Yang X et al (2013) Rock physics model and gas saturation inversion for heterogeneous gas reservoirs. *Chinese Journal of Geophysics Chinese Edition* 56(5):1696–1706
- Yuguang Y, Jian Z et al (2008) Experimental research on the relationship between gas hydrate saturation and acoustic parameters. *Chin J Geophys* 51(4):819–828
- Zhao P, Sun Z, Luo X et al (2016a) Study on the response mechanisms of nuclear magnetic resonance (NMR) log in tight oil reservoirs. *Chin J Geophys* 2016(29):1927–1937. <https://doi.org/10.6038/cjg20160535> (in Chinese abstract)
- Zhao P, Mao Z, Huang Z et al (2016b) A new method for estimating total organic carbon content from well logs. *AAPG Bull* 100(8):1311–1327
- Zhao P, Wang Z, Sun Z et al (2017) Investigation on the pore structure and multifractal characteristics of tight oil reservoirs using NMR measurements: Permian Lucaogou formation in Jimusaer sag, Junggar Basin. *Mar Pet Geol* 2017(86):1067–1081
- Zhao P, Jinhua F, Shi Y et al (2020) Hydrocarbon saturation in shale oil reservoirs by inversion of dielectric logs. *Fuel* 2020(266):116934
- Zhu L, Zhang C, Zhang C, Wei Y, Zhou X, Cheng Y, Huang Y, Zhang L (2018) Prediction of total organic carbon content in shale reservoir based on a new integrated hybrid neural network and conventional well logging curves. *J Geophys Eng* 15(3):1050–1061